Defence Science Journal, Vol. 64, No. 2, March 2014, pp. 159-167, DOI : 10.14429/dsj.64.4659

A Dorsal Hand Vein Recognition-based on Local Gabor Phase Quantization with Whitening Transformation

K. Premalatha*, T. Anantha Kumar, and A.M. Natarajan

Bannari Amman Institute of Technology, Sathyamangalam–638 401, India
**E-mail: kpl_barath@yahoo.co.in*

ABSTRACT

The hand vein pattern is a biometric feature in which the actual pattern is the shape of the vein network and its characteristics are the vein features. This paper investigates a new approach for dorsal hand vein pattern identification from grey level dorsal hand vein information. In this study Gabor filter quadrature pair is employed to compute locally in a window for every pixel position to extract the phase information. The phases of six frequency coefficients are quantized and it is used to form a descriptor code for the local region. These local descriptors are decorrelated using whitening transformation and a histogram is generated for every pixel which describes the local pattern. Experiments are evaluated on North China University of Technology dorsal hand vein image dataset with minimum distance classifier and the results are analyzed for recognition rate, run time and equal error rate. The proposed method gives 100 per cent recognition rate and 1 per cent EER for fusion of both left and right hands.

Keywords: Dorsal hand vein, gabor filter, phase quantization, decorrelation, whitening transformation

1. INTRODUCTION

1.1 Hand Vein Biometrics

Biometrics is the study of techniques for measuring features of living entity that can be used to determine the individual identity. Choi[1] and Badawi[2] state that the vein pattern is a unique property of each individual in the hand. The whole physical arrangement of blood vessels, veins and capillaries within the human body is considered to be different for each individual[3]. The uniqueness of veins in the hand is sparse. The mechanisms underlying the development of the vascular system and the studies on the spatial arrangement of the final vascular network could provide more insight into the probability that no vein pattern will be the same between two individuals.

The hand vein biometric system acquires a vein image which can be taken only at live body, thus the vein image at non-live hand cannot be taken. It extracts the vein pattern inside a hand rather than the outside features of a human body. It is also a good alternative to biometric systems that require physical contact because it extracts the vein pattern, the hand is not in contact with the device instead hand is just easily stretched and the capturing of vein pattern is completed. Due to non-contact, it is hygienic. Since the system has got the three features live body, internal features and non-contact, there is no forgery, and no misuse by evildoers, thus it grasps high security status and can be used at high level security places.

1.2 Literature Review

Daugman[4] discovered that simple cells in the visual cortex of mammalian brains can be modeled by Gabor functions. The image analysis of the Gabor functions is similar to perception in the human visual system. The frequency and orientation representations of Gabor filters are similar to those human visual systems. Gabor filters are found to be particularly appropriate for texture representation and discrimination. In the spatial domain, a 2-D Gabor filter is a Gaussian kernel function modulated by a sinusoidal plane wave. The Gabor filters are self-similar: all filters can be generated from one mother wavelet by dilation and rotation.

Tanaka and Kubo[5] developed a hand vein acquisition device using near IR imaging and employed fast Fourier transform based phase correlation scheme for user verification tested with noise reduction filters, sharpness filters and histogram manipulation. Shahin[6], *et al.* presented fast spatial correlation of hand vein patterns for recognition. After segmentation and pattern post processing correlation is used to measure identity.

Wang[7], *et al.* proposed local scale invariant feature transform (SIFT) which has practical significance due to its translation and rotation invariance. The hand vein image is preprocessed to remove the background and reduce image noises and the SIFT features are extracted to describe the gradient information of hand vein. Minimum distance classifier is used for matching. Tang[8], *et al.* proposed multi-level keypoint detection and SIFT feature based local matching for hand-dorsa vein recognition. In multi-level keypoint detection approach Harris-Laplace and Hessian-Laplace detectors are combined to localize key points that highlight the more discriminating information. Then SIFT based local matching associates these key points between hand dorsa of the same individual. Huang[9],

Received 4 June 2013, revised 4 March 2014, online published 20 March 2014

et al. make use of oriented gradient maps (OGMs) to represent the hand vein images and SIFT based local matching is then performed to associate the key points between corresponding OGM pairs of the same subject.

Kumar and Prathyusha[10] proposed an approach to authenticate user by triangulation of hand vein images and knuckle shape of information palm dorsa hand vein images. The knuckle tips are used for extraction of ROI. The matching scores are generated from the four topologies of triangulation in the binarized vein structures and from the geometrical features consisting of knuckle point perimeter distances in the acquired images. The weighted score level combination of these two matching scores are used to authenticate the individuals.

Wang[11], *et al.* presented partition local binary pattern (LBP) for hand-dorsa vein recognition. In this work after preprocessing the image is divided into sub-images. LBP features are extracted from all the sub-images Minimum distance classifier is used for identification. Wang and Liao[12] presented the feature code for hand vein recognition. The output of partition LBP is extracted and given as input to back propagation encoder. The orthogonal gold code is selected as the output code for back propagation. Correlation classifier is used as the final classifier. Wang[13], *et al.* proposed feature descriptor in which partition LBP is added with feature weighting and error correction code. Feature weighting reduces the influence of insignificant local binary patterns and error correction code increases the distances between feature classes.

In this study NCUT dataset is used to evaluate the proposed algorithm. During preprocessing the region of interest (ROI) is identified from the hand vein images. In the proposed work the quantized phase of the Gabor filter quadrature pair is computed in local image window at every pixel location. Decorrelation technique is applied on quantized image which enhance the differences found in each pixel of an image. The whitening transform is used for decorrelation. The histogram of decorrelated image is considered as the features for the images. Minimum distance classifier and correlation are used for classification purpose.

2. ROI EXTRACTION OF NCUT HAND DORSA VEIN DATASETS

In this dataset to avoid the major hand vein image registration issue a handle is pre-mounted at the bottom of the device to position the hand[14]. The hand vein images are roughly aligned and differed by slight translations and rotations. Back of the hand vein is captured as an image with a resolution of 640 × 480. A dataset of 2040 hand vein images was acquired under the natural lighting condition. It was named as North China University of Technology hand-dorsa vein dataset or NCUT dataset. In detail, 10 right and 10 left back of the hand vein images were captured from all 102 subjects, aged from 18 to 29, of which 50 were male while 52 were female. As the vein pattern is best defined when the skin on the back of the hand is stretched tight, subjects were asked to clench their fists as acquiring vein patterns.

The image coverage area is larger than the back of the hand as shown in Fig. 1(a). In this work, the image centroid was identified to extract the ROI. Let (x_0, y_0) be the centroid of vein image $f(x, y)$ then

$$x_0 = \frac{\sum_{i,j} i \times f(i,j)}{\sum_{i,j} f(i,j)} \quad (1)$$

$$y_0 = \frac{\sum_{i,j} i \times f(i,j)}{\sum_{i,j} f(i,j)} \quad (2)$$

A square region of size R × R pixels with the centroid as the centre is extracted as the vein image to be processed. To confirm the size, ROI with R ranging from 300 pixels to 420 pixels are extracted as shown in Fig. 1.

From Fig. 1 when R = 360 pixels, almost all the hand-dorsa vein information is included. The redundant background information with little hand information is introduced when R = 380 pixels, R = 400 pixels and R = 420 pixels. Therefore 360 × 360 is introduced in this work.

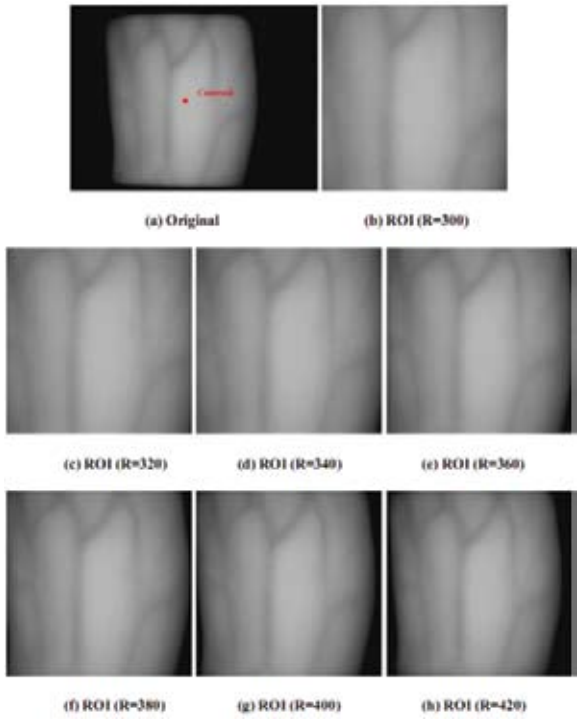

Figure 1: Result of ROI extraction

3. LOCAL GABOR PHASE QUANTIZATION

The most important method for image representation and analysis is the spatial frequency transform, which can be represented in terms of magnitude and phase. Phase is highly invulnerable to noise and contrast distortions and it is an important feature desirable in image processing. The phase in image can be represented by global phase. The global Fourier analysis provides information on the frequency contents of the whole image. Since the content of an image is not stationary, therefore localized frequency analysis has become important in image representation[15].

The discrete model for spatially invariant blurring of an original image $f(x)$ resulting in an observed image $g(x)$ can be

expressed by a convolution given by

$$g(x) = (f * h)(x) \tag{3}$$

where * denotes 2-D convolution, $h(x)$ is the point spread function (PSF) of the blur, and x is a vector of coordinates $[x, y]^T$. In the Fourier domain, this corresponds to

$$G(u) = F(u).H(u) \tag{4}$$

where $G(u)$, $F(u)$ and $H(u)$ are the discrete Fourier transforms (DFT) of the blurred image $g(x)$, the original image $f(x)$, and the $h(x)$ respectively, and u is a vector of coordinates $[u, v]^T$. The magnitude and phase parts of the above equation are separated by

$$|G(u)| = |F(u)|.|H(u)| \tag{5}$$

$$\angle G(u) = \angle F(u) + \angle H(u) \tag{6}$$

The local phase quantization is based on the blur invariance property of the Fourier phase spectrum. It uses the local phase information extracted using the Short-Term Fourier Transform (STFT) computed over a rectangular M × M neighbour hood N_x at each pixel position x of the image $f(x)$ defined by

$$F(u,x) = \sum_{y \in \epsilon_x} f(x-y) e^{-j2\pi u^T y} = z_u^T f_x \tag{7}$$

where z_u is the basis vector of the 2-D discrete Fourier transform at frequency u, and f_x is another vector containing all M^2 image samples from N_x. An efficient way of implementing the STFT is to use 2-D convolutions $f(x) * e^{-j2\pi u^T y}$ for all u. Since the basis functions are separable, computation can be performed using 1-D convolutions for the rows and columns successively.

The analysis of the combined spatial-frequency space can be achieved using various tools, such as short time fourier transform (STFT), gabor transform (GT) and wavelets transform. In the proposed work STFT is computed in local image windows of a preselected form Gabor filter quadrature pair (LGPQ).

The formula for Gabor filter is

$$g(x, y; \lambda, \theta, \psi, \sigma, \gamma) = \exp\left(-\frac{x'^2 + \gamma^2 y'^2}{2\sigma^2}\right) \exp\left(i\left(2\pi \frac{x'}{\lambda} + \psi\right)\right) \tag{8}$$

where $x' = x\cos\theta + y\sin\theta$, $y' = -x\cos\theta + y\sin\theta$, λ is a wavelength of the sinusoidal factor, θ is an orientation of the normal to the parallel stripes of a Gabor function, ψ is a phase offset, σ is a sigma of the Gaussian envelope and γ is the spatial aspect ratio.

It is mostly useful while making derivatives of an image rather than differentiating on the raw signal that should be obtained from the smoothed image. A quadrature pair is a set of two linear operators with the same amplitude response but phase responses shifted by 90 degrees. Quadrature pairs measure local oriented energy. These can be used to identify contours, independently of the phase of the contour. Gabor filter quadrature pair in spatial domain converted into the frequency domain by taking the Fourier transform. Fourier transform transforms the measured k-space data into image space and the image data is a complex type. The complex argument of a complex number is called as phase.

In LGPQ six complex coefficients are considered corresponding to 2-D frequencies $u_1 = [b,0]^T$, $u_2 = [0,b]^T$, $u_3 = [b,b]^T$, $u_4 = [b,-b]^T$, $u_5 = [-b,-b]^T$ and $u_6 = [-b,b]^T$ where b is a scalar frequency. Let

$$F(x) = \left[F(u_1,x),\ F(u_2,x),\ F(u_3,x),\ F(u_4,x), F(u_5,x), F(u_6,x)\right] \tag{9}$$

$$G(x) = \left[real\{F(x)\}, img\{F(x)\}\right]^T \tag{10}$$

where real{.} and img{.} return real and imaginary parts of a complex number respectively. The corresponding 12-by-M^2 transformation matrix is

$$Z = \left[\text{real}\{z_{u1} z_{u2} z_{u3} z_{u4} z_{u5} z_{u6}\}, \text{img}\{z_{u1} z_{u2} z_{u3} z_{u4} z_{u5} z_{u6}\}\right]^T \tag{11}$$

So that $G(x) = Zf_x$

Window size determines the locality of the quantized phase. Increasing the window size will result in a further degradation of the original signal, as more features located in each window will be affected. Increasing quantization will reduce the feature (edge) degradation on one hand, and reduce the energy of the signal on the other hand. The number of quantization levels is in between 2 and ∞.

In the proposed work the LGPQ descriptor is formed locally for every pixel. The STFT coefficients are computed in the M × M neighbour hood of the pixel for the lowest horizontal, vertical, and diagonal frequencies (1,0), (0,1), (1,1), (1,-1), (-1,-1) and (-1,1). Real and imaginary parts of these six frequencies are binary quantized based on their sign. If it is greater than 0 then the corresponding quantized value is 0 otherwise 1.

$$q_j = \begin{cases} 1, & if\ g_j \geq 0 \\ 0, & otherwise \end{cases} \tag{12}$$

where g_j is the j^{th} component of $G(x)$. The quantized coefficients are represented as integer values between 0-4095 using binary coding

$$b = \sum_{j=1}^{12} q_j 2^{j-1} \tag{13}$$

3.1 Decorrelation with Whitening Transformation

Before quantization the coefficients are decorrelated, because it is shown that the information is maximally preserved in scalar quantization if the samples to be quantized are statistically independent[15]. A whitening transformation is a decorrelation transformation that transforms a set of random variables having a known covariance matrix M into a set of new random variables whose covariance is the identity matrix. The transformation is called whitening because it changes the input vector into a white noise vector.

The inverse colouring transformation transforms a vector Y of uncorrelated variables (a white random vector) into a vector Z with a specified covariance matrix. Suppose Z is a random vector with covariance matrix M and mean 0. The matrix M can be written as the expected value of the outer product of Z by itself, namely

$$M = \mathrm{E}[ZZ^T] \tag{14}$$

since M is symmetric and positive semi definite, it has a square root $M^{1/2}$, such that $M^{1/2}(M^{1/2})^T = M$. If M is positive definite, $M^{1/2}$ is invertible. Then the vector $Y = M^{-1/2}Z$ has covariance matrix:

$$Cov(Y) = \mathrm{E}[YY^T] = M^{-1/2}\mathrm{E}[ZZ^T](M^{-1/2})^T \tag{15}$$

$$Cov(Y) = M^{-1/2}M(M^{-1/2})^T = (M^{-1/2}M^{1/2})((M^{1/2})^T(M^{-1/2})^T) = I \tag{16}$$

and is therefore a white random vector. Since the square root of a matrix is not unique, the whitening transformation is not unique either. If M is not positive definite, then $M^{1/2}$ is not invertible, and it is impossible to map Z to a white vector of the same length. In that case the vector Z can still be mapped to a smaller white vector Y with m elements, where m is the number of non-zero eigenvalues of M.

The covariance matrix of the transform coefficient vector F_x can be obtained from $M = E(ZZ^T)$ If the data points in Z are correlated, then their covariance M will not be a diagonal matrix. In order to decorrelate the data, the data need to be transformed and the transformed data will have a diagonal covariance matrix. This transform can be done by using the eigenvalue problem.

Thus, the data have been decorrelated: its covariance is now a diagonal matrix. The diagonal elements (eigenvalues) may be the same or different. If they are same then it is called whitening the data. Each eigenvalue determines the length of its associated eigenvector; the covariance will correspond to an ellipse when the data is not whitened. The covariance will correspond to a sphere and all dimensions have the same length, or uniform when the data is whitened.

The uniform phase shift to all vectors happens due to the whitening transform it makes the coefficient vectors are subject to a twelve dimensional rotation. The twelve dimensional spaces are divided into 4096 hypercubes during quantization. Based on the phase information the vector is assigned to one of these hypercubes.

Figure 2 shows the LGPQ method which illustrates the computation of LGPQ code for the gray pixel using 5 × 5 neighbourhood at 6 frequency levels. The histogram is obtained by adding the LGPQ code at every pixel position after decorrelation with whitening transformation.

4. EXPERIMENT RESULT ANALYSIS

The biometric authentication system compares enrolled biometric data with the identity of the person claimed if the matching is closer, then the match score is higher. If the match score exceeds a given threshold then the person authenticating is accepted. The system will generate two types of errors called the false negative rate (FNR) and the false positive rate (FPR). Both FPR and FNR depend on a threshold. A higher threshold will generally reduce FPR, but at the expense of increased FNR, and vice versa. The threshold affects FNR and FPR. At a low threshold FNR will be low and FPR will be high. When the threshold is increased more genuine users will be rejected and fewer impostors will be accepted. At some point FNR and FPR will be equal. The value of the FPR and FNR at this point is the equal error rate (EER). The EER tells about what the FPR and FNR will be at any other threshold. Sensitivity is also called as true positive rate (TPR) or the Recall rate. It measures the proportion of actual positives which are correctly identified. Specificity measures the proportion of negatives which are correctly identified as such.

Receiver operating characteristic (ROC) curve plots parametrically the FPR (i.e. imposter attempts is accepted) on the x-axis, against the corresponding TPR (i.e. genuine attempts accepted) on the y-axis as a function of the decision threshold. As the match threshold raised both detection and false alarms decrease. In biometric system these conflicting rates must be balanced to find an acceptable operating point and each point in ROC represents a possible combination. A detection error trade-off (DET) curve plots error rates on both axes, giving uniform action to both types of error[16]. The DET curves can be used to plot matching error rates FNR against FPR. The cumulative match curve (CMC) is used as a measure of 1:m identification system performance. It is used to discover the ranking capabilities of an identification system.

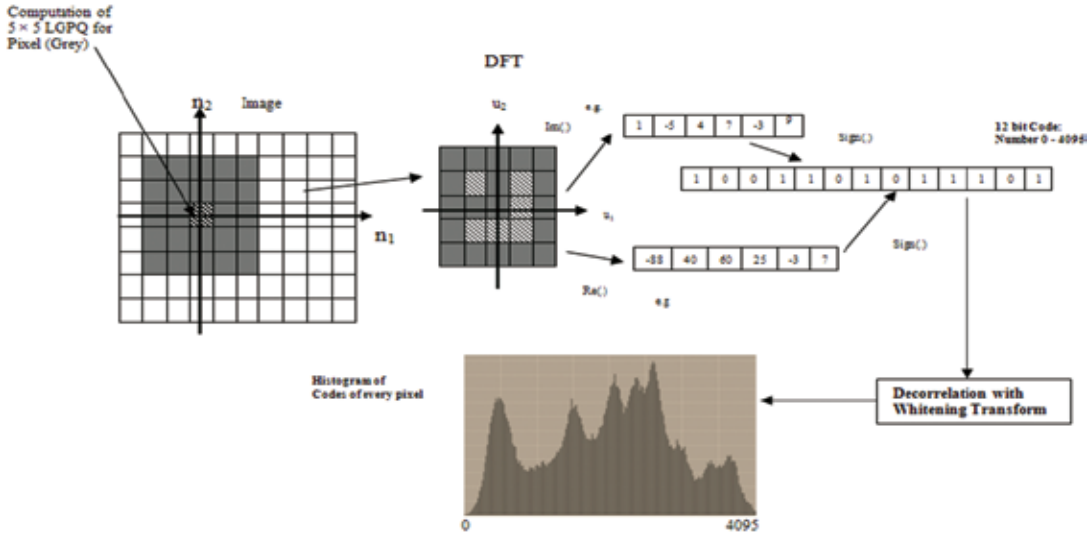

Figure 2. The LGPQ with Whitening Transformation.

The CMC curve gives the graphical presentation of results of an identification task test, it plots rank values on the x-axis and the probability of correct identification at or below that rank on the y-axis.

In the proposed work LGPQ is used for texture classification and the 12 bit code for every image pixel is added to create a 4095 bin histogram which describes the texture. Texture classification is then carried out based on the distance between the histograms, example, using the Chi square distance measure with the minimum distance classifier. The chi-square distance hinges in the widespread use of the goodness of fit test as one of the most common for statistical conformity

The proposed system evaluates its performance in NCUT dataset. For classification the minimum distance classifier is used to classify the test image data to classes which minimize the distance between the training image data and the class in feature space. To compare the histogram distance measure is used. The distance is defined as an index of similarity, so that the minimum distance is identical to the maximum similarity. The following distance measures are used to identify the distance between two histograms.

$$\text{Euclidean distance : } d(p,q)=\sqrt{\sum_i (p_i - q_i)^2} \quad (17)$$

$$\text{City block distance : } d(p,q)=\sum_i |p_i - q_i| \quad (18)$$

$$\text{Minkowski distance: } d(p,q)=\left(\sum_i |p_i - q_i|^n\right)^{\frac{1}{n}} \quad (19)$$

$$\text{Chi square : } \chi^2(p,q)=\sum_i \frac{(p_i - q_i)^2}{p_i + q_i} \quad (20)$$

where p and q represent the individual histogram bin values.

4.1 NCUT Dataset

The experiments are done on left hand vein images, right hand vein images and both the left and right hand vein images. Since vein patterns of both hands of the same person are naturally different to some level[16] the left and right dorsal hands of a person should have complementary information for recognition. To estimate the generalisation error k fold cross-validation is applied[17]. The 10 samples of 102 subjects are divided into 5 equal parts. The classification model is trained on 4 parts and tested on the remaining one part. This is performed 5 times and the average error over the 5 runs is considered as an estimate of the generalization error. Table 1 shows the recognition rate and run time of NCUT left dorsal hand dataset, right dorsal hand dataset and both fusion for chi-square test and 3 different distance measures. The chi-square test outperforms other distance measures city block, Euclidean and Minkowski both in recognition rate and computational time. By considering the hands the fusion of both dorsa hands outperforms single dorsa hand vein and it gives 100 per cent results for chi square and Euclidean distance measures.

The proposed work was tested in favour of limited sample images per person enrollment. This is due to the difficulties of sample collection or the blockage of storage capability of the systems. Therefore the test is made on by varying the size of gallery samples of each person from 1 to 9. For each size of the training data set with the number of images used increasing from 1 to 9 (N_T = 1, 2,3…, 9) 10 tests were performed with the training samples selected randomly in each test. Obviously, as the number of training images increases, the number of images available for test is decreased, and the recognition performance has improved with more time required for computation. Table 2 shows that the recognition rate of LGPQ is generally improved as the gallery size increases and the proposed work can achieve a recognition rate of 97.79 per cent for chi-square when only one sample is enrolled in the gallery set of each subject for both hands.

Figure 3 shows (a) ROC curve, (b) DET curve, and (c) CMC curve obtained from the fusion of left and right hand dorsa vein for Euclidean, Cityblock, Minkowski and Chi-square measures. In ROC the more bowed the curve is towards the upper left corner, the better the classifier's ability to discriminate between the pattern classes. DET curve helps to indicate the performance of the system by plotting false match rate against the false non-match rate for a range of score thresholds. This will also estimate the widely used equal error rate (EER) which is the point at which the false match rate is equal to the false non-match rate. Figure 4 shows the EER obtained from Chi-square, Cityblock, Euclidean, and Minkowski for fusion of both hands. EER curve plots the FAR and the FRR on the vertical axis against the threshold score on the horizontal axis. The point of intersection of these two curves is the EER, i.e. when the false acceptance rate is equal to the false rejection rate. Table 3 shows EER obtained from a left hand dorsa vein, right hand dorsa vein and fusion of both. The

Table 1. Recognition rate and run time for NCUT Hand-Dorsa vein dataset

Distance measure	Chi - square		City block		Euclidean		Minkowski	
Dataset	Recognition rate (%)	Time (s)	Recognition rate (%)	Time (s)	Recognition rate (%)	Time (s)	Recognition rate (%)	Time (s)
Left hand	99.71	0.073	99.60	0.113	98.23	0.113	96.18	0.181
Right hand	99.71	0.069	99.31	0.560	98.62	0.113	96.27	0.180
Both hand	100.00	0.090	100.00	0.140	98.92	0.141	97.94	0.220

Table 2. Recognition rate (%) of using different number of training images

Training images	Test images	Chi-square			Cityblock			Euclidean			Minkowski		
		Left hand	Right hand	Both hands	Left hand	Right hand	Both hands	Left hand	Right hand	Both hands	Left hand	Right hand	Both hands
1	1836	93.30	94.39	97.79	92.12	93.95	96.22	78.52	79.84	85.98	67.07	71.02	75.20
2	1632	96.22	95.83	98.04	95.24	94.47	97.69	91.72	89.58	91.68	84.77	88.45	91.43
3	1428	97.47	98.04	99.44	96.91	97.33	99.15	92.01	92.71	93.69	85.71	90.09	92.97
4	1224	98.36	99.02	100.00	98.04	98.36	99.51	94.43	95.75	97.54	88.88	92.15	92.97
5	1020	98.82	99.02	100.00	98.82	99.02	99.80	96.86	95.68	98.62	92.15	92.74	96.07
6	816	99.02	99.02	100.00	99.01	99.02	99.75	97.05	96.32	98.77	94.60	94.36	96.07
7	612	99.67	100.00	100.00	99.67	100.00	100.00	98.36	99.01	99.34	95.09	96.40	97.71
8	408	99.51	100.00	100.00	99.51	100.00	100.00	98.04	99.51	99.01	94.60	97.54	98.03
9	204	100.00	100.00	100.00	100.00	100.00	100.00	99.01	100.00	100.00	94.11	96.07	98.03

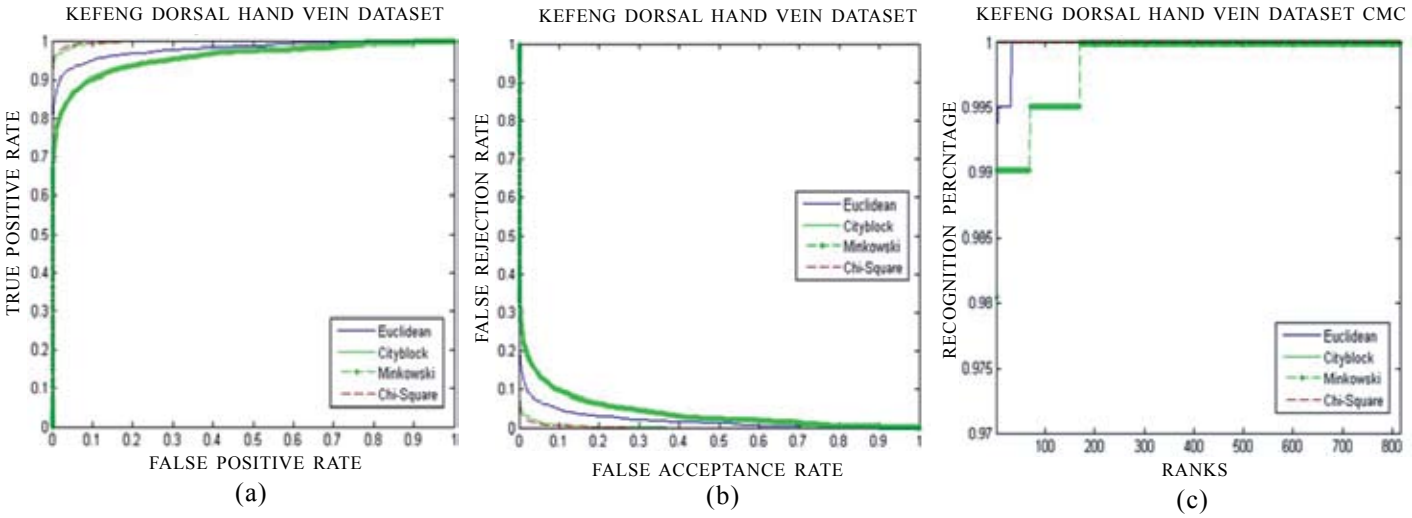

Figure 3. (a) ROC, (b) DET, and (c) CMC curve for fusion of both hands.

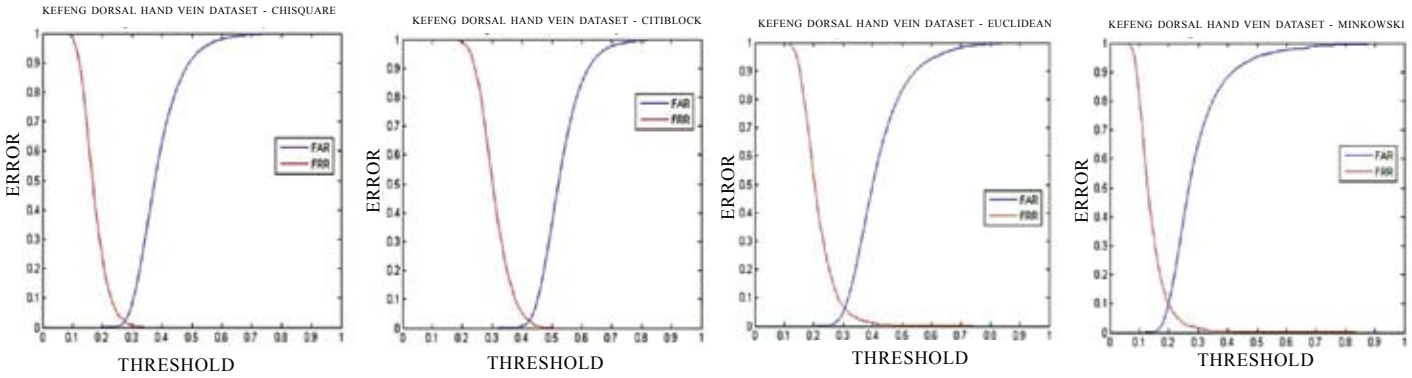

Figure 4. EER curve for fusion of both hands.

Table 3. Equal error rate

Distance measure	Equal error rate		
	Left	Right	Fusion
Chi-Square	0.035	0.025	0.010
Cityblock	0.050	0.030	0.025
Euclidean	0.090	0.080	0.050
Minkowski	0.120	0.110	0.095

lower the EER value, the higher the accuracy of the biometric system. Fusion with chi-square gives the lowest value.

Table 4 shows the performance of different methodologies for distinct hand dorsa vein images.

5. CONCLUSION

In this paper LGPQ is proposed that operates on the Fourier phase local window in every image position. The phases of the six low-frequency coefficients are uniformly quantized with whitening transformation into one of 4095 hypercubes in 12 dimensional spaces; it gives a twelve bit code. These codes for all image pixel neighbour hoods are collected into a histogram bin, which can be used for classification. The NCUT dataset is used for analysis and the minimum distance classifier is used for classification. Among the distance measures the chi square outperforms both in recognition rate and run time. A fusion of both hands gives 100 per cent recognition rate for chi square and Euclidian distance measure and it gives 1 per cent EER for chi-square distance measure. The results are also analyzed for gallery of images due to the complicatedness of sample collection. The leave one out cross validation gives

Table 4. Performance of different methodologies

Reference	Methodology	Imaging	Number of subjects	Samples for each subject	Total images	Performance (%)
Cross and Smith[18]	Sequential correlation in vein maps	NIR, HDF	20	5	100	FAR = 0 FRR = 7.9
Im[19], *et al.*	DSP processor	NIR imaging	Not mentioned	Not mentioned	5000	FAR = 0.001 Reliability = 99.45
Tanaga and kubo[5]	FFT based phase correlation	NIR,HDF	25	Not mentioned	Not mentioned	FAR = 0.073 FRR = 4
Fan[20], *et al.*	Multi-resolution analysis and combination	Thermal hand vein imaging	32	30	960	FAR = 3.5 FRR = 1.5
Wang and Leedham[21]	Line Segment Housdorff distance matching	Thermal hand vein imaging	12	9	108	FAR = 0 FRR = 0
Ding[22], *et al.*	Distance between feature points	NIR imaging,	48	5	240	FAR = 0 FRR = 0.9
Shahin[6], *et al.*	fast spatial correlation	NIR imaging	50	10	500	EER = 0.25
Wang[23], *et al.*	A multi-resolution wavelet algorithm	NIR imaging	82	10	820	FAR = 0.046 FRR = 5.08
Wang[24], *et al.*	Modified Hausdorff distance algorithm	Far-infrared imaging	47	3	141	EER = 0
Kumar and Prathyusha[10]	Vein triangulation and knuckle tips	NIR imaging	Not mentioned	Not mentioned	100	FAR = 1.14 FRR = 1.14
Wang[7], *et al.*	SIFT	NIR imaging	102	20	2040	FAR = 0.002 FRR = 0.93 .
Wang[11], *et al.*	LBP	NIR imaging	102	20	2040	Recognition rate = 8.13
Crisan[25], *et al.*	Thinning algorithm	NIR imaging	306	2	612	FAR = 0.012 FRR = 1.03
Huang[9], *et al.*	Oriented gradient maps	NIR imaging	102	20	2040	Recognition rate = 7.60
Wang and Liao[12]	LBP with back propagation encoder	NIR imaging	102	20	2040	Recognition rate = 7.60
Wang[13], *et al.*	Coded and weighted LBP	NIR imaging	102	20	2040	Recognition rate = 8.63
Authors	LGPQ with whitening transformation	NIR imaging	102	20	2040	Recognition rate = 100 EER =1

97.79 per cent recognition rate for both hands in chi square. The experimental results are also examined with SIFT, LBP variants and oriented gradient maps for this NCUT data set. The LGPQ gives 100 per cent recognition rate and it outperforms the existing methods.

ACKNOWLEDGEMENT

This work is supported by the research grant from Defence Research and Development Organization (DRDO), Government of India, New Delhi, grant no. ERIPR/ER/0903931/M/01/1321.

Portions of the research in this paper use the NCUT Hand-dorsa Vein Database collected by North China University of Technology, China.

REFERENCES

1. Choi, H.S. Apparatus and method for identifying individuals through their subcutaneous vein patterns and integrated system using said apparatus and method. US Patent No. 6301375, 9 October 2001.
2. Badawi, Ahmed M. Hand vein biometric verification prototype: A testing performance and patterns similarity. *In* the Proceedings of the International Conference on Image Processing Computer Vision and Pattern Recognition, Las Vegas, Nevada, USA, 2006.
3. Willmore, M.R. Infra-red imaging and pattern recognition system. US Patent No. 5351303, 27 September 1994.
4. Daugman, J.G. Complete discrete 2-D gabor transforms by neural networks for image analysis and compression. *IEEE T. Acoust. Speech*., 1988, **36**(7), 1169 -79.
5. Tanaka, T. & Kubo, K. Biometric authentication by hand vein patterns. *In* the Proceedings of SICE Annual Conference. Yokohama, Japan, 2004.
6. Shahin, M.; Badawi, A. & Kamel, M. Biometric authentication using fast correlation of near infrared hand vein patterns. *Int. J. Biomed. Sci.*, 2007, **2**(3), 141-148.
7. Wang, Y.; Wang, D.; Liu, T. & Li, X. Local SIFT analysis for hand vein pattern verification. *In* the Proceedings of the SPIE International Conference on Optical Instruments and Technology: Optoelectronic Information Security. Shanghai, China, 2009.
8. Tang, Y.; Huang, D. & Wang, Y. Hand-dorsa vein recognition based on multi-level keypoint detection and local feature matching. *In* the Proceedings of the 21st International Conference on Pattern Recognition. Tsukuba, Japan, 2012.
9. Huang, D.; Tang, Y.; Wang, Y. & Chen, L. Hand vein recognition based on oriented gradient maps and local feature matching. *In* the Proceedings of the 11th Asian Conference on Computer Vision. Verlag, Berlin Heidelberg, 2012.
10. Ajay Kumar, K. & Prathyusha, K. Personal authentication using hand vein triangulation and knuckle shape. *IEEE T. Image Process*., 2009, **38**(9), 2127-36.
11. Wang, Y.; Li, K. & Cui, J. Hand-dorsa vein recognition based on partition local binary pattern. *In* the Proceedings of 10th IEEE International Conference on Signal Processing. Beijing, China, 2010.
12. Wang, Y. & Liao, W. Hand vein recognition based on feature coding. *In* the Proceedings of the 7th Chinese conference on Biometric Recognition. Guangzhou, China, 2012.
13. Wang, Y.; Li, K.; Shark L.K. & Varley MR. Hand-dorsa vein recognition based on coded and weighted partition local binary patterns, *In* the Proceedings of International Conference on Hand based Biometrics. Hong Kong, China, 2012.
14. Zhao, S.; Wang, Y. & Wang, Y. Biometric identification based on low quality hand vein pattern images. *In* the Proceedings of the 7th International Conference on Machine Learning and Cybernetics. Kunming, China, 2008.
15. Ojansivu, V. & Heikkila, J. Blur insensitive texture classification using local phase quantization. *In* the Proceedings of 3rd International Conference on Image and Signal Processing. Berlin, Germany, 2008.
16. Kohavi, R. A study of cross-validation and bootstrap for accuracy estimation and model selection. *In* Proceedings of the 14th International Joint Conference on Artificial Intelligence. Montreal, Quebec, Canada, 1995.
17. Martin, A.; Doddington, G.R.; Kamm, T.; Ordowski, M. & Przybocki, M.A. The DET curve in assessment of detection task performance. *In* the Proceedings of Eurospeech. Rhodes, Greece, 1997.
18. Cross, J.M. & Smith, C.L. Thermo graphic imaging of the subcutaneous vascular network of the back of the hand for biometric identification. *In* the Proceedings of the 29th Annual International Carnahan Conference on Security Technology. Sanderstead, London, 1995.
19. Kim, S.; Park, H.M.; Kim, Y.W.; Han, S.C.; Kim, S.W. & Hang, C.H. An biometric identification system by extracting hand vein patterns. *J. Korean Phys. Soc.*, 2001, **38**(3), 268-72.
20. Fan, K.C. & Lin, C.L. Biometric verification using thermal images of palm-dorsa vein patterns. *IEEE T. Circ. Syst. Vid*., 2004, **14**(2), 199 - 213.
21. Wang, L. & Leedham, C.G. A thermal vein pattern verification system. *In* the Proceedings of International Conference on Advances in Pattern Recognition. Bath, UK, 2005. pp. 58-65.
22. Ding, Y.; Zhuang, D. & Wang, K. A study of hand vein recognition method. *In* the Proceedings of IEEE International Conference on Mechatronics and Automation. Niagara Falls, Canada, 2005.
23. Wang, L.; Leedham, G. & Cho, D.S. Minutiae feature analysis for Infrared hand vein pattern biometrics. *Pattern Recogn.*, 2008a, **41**(3), 920-29.
24. Wang, Y.; Liu, T. & Jiang, J. A multi-resolution wavelet algorithm for hand vein pattern recognition. *Chin. Opt. Lett*., 2008b, **6**(9), 657-60.
25. Crisan, S.; Tarnovan, I.G. & Crisan, T.E. Radiation optimization and image processing algorithms in the identification of hand vein patterns. *Comp. Stand. Inter.*, 2010, **32**(3), 130–40.

CONTRIBUTORS

Dr K. Premalatha did her ME and BE in Computer Science and Engineering at Bharathiar University, Coimbatore, Tamil Nadu and PhD (Computer Science and Engineering) at Anna University, Chennai, India. Currently she is working as a Professor in the Department of Computer Science and Engineering at Bannari Amman Institute of Technology, Erode, Tamil Nadu, India. Her research interests include data mining, image processing, information retrieval and soft computing.

Mr T. Anantha Kumar received his BE (Computer Science and Engineering) from Anna University, Chennai in 2006 and ME (Computer Science and Engineering) from Anna University of Technology, Coimbatore in 2009. He is currently working as a Senior Research Fellow at Bannari Amman Institute of Technology, Erode, Tamil Nadu, India. His areas of interest include image processing, data mining and optimization techniques.

Dr A.M. Natarajan received his BE, MSc and PhD from the PSG College of Technology, Coimbatore, India. He is currently working as Chief Executive at Bannari Amman Institute of Technology, Erode, Tamilnadu, India. He had published more than 70 papers in National and International Journals and He authored and published 10 Books. His research areas of interest include image processing, data mining and soft computing.